Some Design Aspects of an Absorbing 3D Wavemaker

Hemming A. Schäffer[1]

ABSTRACT

A new absorbing multidirectional wavemaker is under development at the Danish Hydraulic Institute. In this process numerous aspects of the design and control of multielement wavemakers as well as the theory for wave generation and active absorption have been considered. This paper focuses on two specific and specialized points. First, the influence of finite segment width on the wave field generated is analysed for different types of paddle front. In this connection a new criterion for the truncation of directional spectra to be generated is suggested. Second, the appearance and reduction of aliasing problems for 3D active absorption is discussed. Aliasing appears due to the spatial sampling typically used for obtaining a hydrodynamic feedback in the absorption procedure.

INTRODUCTION

A traditional wavemaker is controlled independently of the waves present in its vicinity. Thus, if the waves generated by the wavemaker are reflected from some boundary or construction in the flume or basin, then full re-reflection takes place when these waves return to the wavemaker. The result is an undesirable distortion of the incident wave field.

An absorbing wavemaker attempts to eliminate this problem by including some hydrodynamic feedback signal in the paddle control. Simultaneously with the usual wave generation, reflected waves are absorbed by moving the paddle appropriately.

Absorbing wavemakers for wave flumes are now routinely used in a number of laboratories. For multidirectional wavemakers the simplest option is to use independent absorption control systems for each wavemaker segment. This gives a quasi-3D system, which does not account for wave obliqueness in the absorption procedure. Nevertheless, a quasi-3D system provides a significant improvement over a traditional segmented wavemaker. In very recent years, fully 3D systems have been pursued. Wave obliqueness is accounted for through a coupling between the control of neighbouring paddle segments. For a review of active absorption methods with emphasis on 3D systems, see Schäffer and Klopman (1997).

---

[1] Danish Hydraulic Institute, Agern Allé 5, DK-2970 Hørsholm, Denmark, e-mail: has@dhi.dk

At the last ICCE, we presented a fully 3D theory for active absorption of multidirectional waves (Schäffer and Skourup, 1996). Within the framework of linear waves, this theory was developed in the wavenumber-frequency domain (k_y, ω), using the wavenumber component along the wavemaker. The result was a 2D transfer function $F(k_y, \omega)$, relating the amplitude of the wavemaker position $X_a(k_y, \omega)$ to the amplitude of the surface elevation measured along the wavemaker $A(k_y, \omega)$. The same transfer function appeared in the combined generation/absorption problem. Phase relations were accounted for, since F, X_a and A were complex. In order to obtain a physically realisable representation, a 2D digital recursive filter was developed. This filter was designed to have a transfer function approximating $F(k_y, \omega)$, thus giving the wavemaker paddle position $X(m\Delta y, n\Delta t)$ as output when provided with the surface elevation $\eta_0(m\Delta y, n\Delta t)$ measured along the wavemaker as input. Here, y is the coordinate along the wavemaker and t is time. The space-time domain was sampled at $(y,t) = (m\Delta y, n\Delta t)$ where Δy equals the individual paddle width of the segmented wavemaker. A wave elevation gauge was assumed to be mounted on each segment. Schäffer and Skourup tested the absorption algorithm in a numerical wave tank based on the Boundary Integral Equation Method and concluded that the system gave a significant improvement over a quasi-3D system.

One of the shallow water facilities at Danish Hydraulic Institute is now being upgraded with a multidirectional wavemaker and the active absorption system is an important part of this development. The new wavemaker is scheduled to be ready in 1999 and thus the practical performance of the system will be published at a later occasion. The present paper reports a number of investigations made in connection with the design of the multidirectional wavemaker front.

SELECTED DESIGN CONSIDERATIONS

The active absorption depends on the elevation measured directly on the paddle front of the wavemaker. This makes the local wave field very important and it gives a renewed interest in phenomena like evanescent modes and spurious wave generation due to finite paddle width. Since the surface elevation is measured at discrete points in space, aliasing problems must also be considered.

Spurious Waves and Evanescent Modes for Different types of paddle front
The finite spatial resolution Δy of a segmented wavemaker results in spurious waves (see eg Sand, 1979). Let the wavelength along the wavemaker be $L_y = 2\pi/|k_y|$ and let the wave direction be θ then if $L_y / \Delta y > \sin|\theta|/(1 + \sin|\theta|)$, these appear only as evanescent modes confined to the vicinity of the wavemaker. For high frequencies and large obliqueness, the resolution becomes very coarse, and spurious progressive waves are generated. Since spurious waves in general influence the local wave field and since spurious progressive waves contaminate the whole wave basin, it is interesting to know how large they get. This depends on the variation of the paddle front, and thus we have studied three different types of paddles with a) a constant, b) a linear and c) a cubic spline variation between the discrete points at which the position is controlled. Type a) is often called 'the staircase approximation', while b) is known as a vertically hinged paddle. Type c) requires a flexible paddle and it has probably never been used in practice.

One problem with the flexible paddle is that it needs to be sufficiently rigid to sustain the wave forces. We have estimated that the power required to bend the paddle is consequently in the same order of magnitude as the power required to generate the waves. However, we have

included the flexible paddle in the analysis anyway as it represents the best interpolation one could possibly obtain for this type of problem.

In this paper, we shall refer to the three types of paddle fronts by the shape of their segments, namely as constant, linear and spline elements, respectively. For $L_y/\Delta y = 5$, Fig. 1 shows a sketch for each of the three types of elements in comparison with the sinusoid to be approximated.
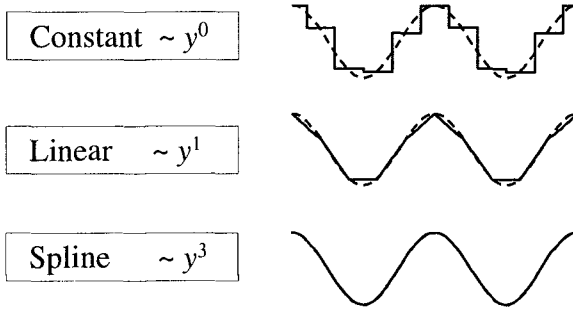

Figure 1. Different types of paddle fronts considered: constant, linear and cubic spline elements. Resolution: $L_y/\Delta y = 5$.

Part of this investigation has been made before (Sand, 1979, types a) and b)), with the emphasis on progressive spurious waves. The purpose of the present analysis is twofold. First, we establish a more elaborate condition than just cutting at $L_y / \Delta y = \sin |\theta| / (1 + \sin |\theta|)$ when truncating a directional spectrum to be generated. The condition suggested limits the amplitude of progressive spurious waves and it depends on the type of wave paddle. This further supports the decision on which paddle type to chose in multidirectional wavemaker design. Second, we calculate the local wave field in detail for use in connection with active absorption.

Let the paddle position, $X(y_m, t)$ be given as a sinusoid with amplitude X_a sampled at equidistant points,

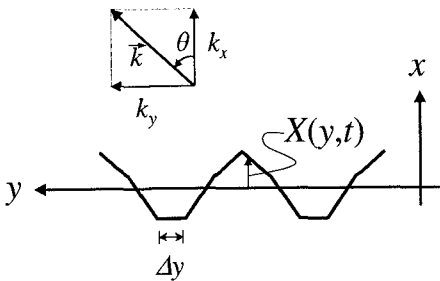$$X(y_m, t) = X_a \exp[i(\omega t - k_y y_m)], \quad y_m = m\Delta y \tag{1}$$

Figure 2. Definition sketch.

see Fig. 2 for a definition sketch. The continuous position, $X(y,t)$ is then determined by the type of paddle front, i.e. the type of interpolation. Generally, we may write

$$X(y,t) = \xi(y)X_a \exp[\omega t], \quad \xi(y_m) = \exp[-ik_y y_m] \tag{2}$$

For constant elements, we have

$$\xi(y) = \xi(y_m), \quad y_{m-1/2} \le y \le y_{m+1/2} \tag{3}$$

For linear and spline elements the interpolation can be written as

$$\xi(y) = A(y)\xi(y_m) + B(y)\xi(y_{m+1}) + \\ + C(y)\xi''(y_m) + D(y)\xi''(y_{m+1}), \quad y_m \le y \le y_{m+1} \tag{4}$$

where

$$A(y) = (y_{m+1} - y)/\Delta y, \quad B(y) = (y - y_m)/\Delta y \tag{5}$$

For spline elements, we get

$$C(y) = \frac{\Delta y^2}{6} A(A^2 - 1), \quad D(y) = \frac{\Delta y^2}{6} B(B^2 - 1) \tag{6}$$

while these cubic terms vanish for linear elements, i.e. $C(y)=D(y)=0$. For the spline case, it may be verified that (3) and (4) ensure continuity in both $\xi(y)$ and $\xi''(y)$ at $y=y_m$. Further requiring that also $\xi'(y)$ is continuous at $y=y_m$ gives a linear system of $N=L_y/\Delta y$ equations relating $\xi''(y_n)$ to $\xi(y_n)$, assuming an integer number of elements per wavelength along the wavemaker. Due to periodicity of the problem, the coefficient matrix involved is circulant, i.e. each row is identical to the previous one except for being rotated one place to the right. Using the Discrete Fourier Transform, this linear system can be solved for any value of N to give

$$\xi''(y_m) = \xi(y_m) 6 \frac{\cos(k_y \Delta y) - 1}{\cos(k_y \Delta y) + 2} \tag{7}$$

It may be shown, that both this and the following results can also be obtained under the assumption that N is a rational number. For continuity reasons we further conjecture that also irrational values of N are allowed. For simplicity, however, we shall maintain the assumption of integer N in the following derivations. Expanding $\xi(y)$ in a Fourier series

$$\xi(y) = \sum_{n=-\infty}^{\infty} a_n \exp[ink_y y], \quad a_n = \frac{1}{L_y} \int_0^{L_y} \xi(y)\exp[-ink_y y]dy \tag{8}$$

it turns out that all but every N'th coefficient vanish, and the remaining ones appear for $n=pN-1$, where p is an integer. The result may generally be expressed as

$$\xi(y) = \sum_{p=-\infty}^{\infty} a_p \exp[-ik_{yp} y], \quad k_{yp} = k_y - pk_{\Delta y}, \quad k_{\Delta y} = \frac{2\pi}{\Delta y} \qquad (9)$$

irrespective of the type of paddle front. After quite some algebra, we get

$$a_p = \begin{cases} \beta_p, & \text{constant elements,} \\ \beta_p^2, & \text{linear elements,} \\ \dfrac{3}{2 + \cos(k_y \Delta y)} \beta_p^4, & \text{spline elements,} \end{cases} \qquad \beta_p = \frac{\sin\left(\dfrac{k_{yp} \Delta y}{2}\right)}{\dfrac{k_{yp} \Delta y}{2}} \qquad (10)$$

where the first two results were given by Sand (1979). It appears that in all three cases the power of β_p equals the order of the interpolating polynomial plus one. The primary component given by $p=0$ represents the desired motion, while all other components are spurious modes due to finite resolution. The perfect sinusoid recovers for $N \rightarrow \infty$ (or $k_y \Delta y \rightarrow 0$) for which $a_0 \rightarrow 1$ and $a_p \rightarrow 0, p \neq 0$. Figure 3a shows $|a_p|$ for $p \in [-2;2]$ versus $1/N = k_y / k_{\Delta y}$ for constant elements. Similar curves are shown in Fig. 3b for linear elements and in Fig. 3c for spline elements, where c_{-1}, c_{-2} and c_2 are hardly visible. While increasing the order of interpolation clearly improves the results when $1/N$ is small, the main spurious component dominates over the primary component for any type of interpolation when the resolution is more coarse than corresponding to the Nyquist limit, i.e. when $1/N>1/2$. This illustrates the importance of resolution and the limited possibility for improvements by high order interpolation. Irrespective of the type of interpolation all paddles move in phase if $1/N=1$ and the wavemaker reduces to a long-crested wavemaker. This is in line with (9), since for $N \rightarrow 1$, we have $k_{y1} \rightarrow 0$, $a_1 \rightarrow 1$ and $a_p \rightarrow 0, p \neq 1$.
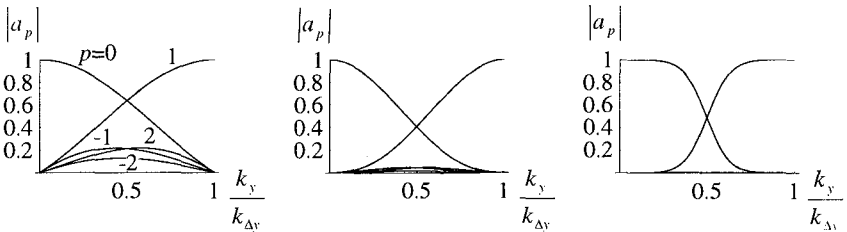

Figure 3. Fourier coefficients $|a_p|$ versus $1/N = k_y / k_{\Delta y}$ for $p \in [-2;2]$. Left plot: constant elements; middle plot: linear elements; right plot: spline elements.

While the above results give an indication on how well the ideal sinusoid is reproduced by a given type of segmentation, it does not show which waves will be generated. Summing up the solution (see e.g. Dean and Dalrymple, 1984) for each sinusoidal paddle mode, the surface elevation of the waves generated by the paddle movement from (9) can be written as

$$\eta(x, y, t) = X_a \sum_{p=-\infty}^{\infty} a_p \sum_{j=0}^{\infty} e_{jp} \exp\left[i(\omega t - k_{xjp} x - k_{yp} y)\right] \tag{11}$$

where

$$e_{jp} = \frac{k_j}{k_{xjp}} c_j, \quad k_{xjp} = \sqrt{k_j^2 - k_{yp}^2}, \quad \omega^2 = g k_j \tanh k_j h \tag{12}$$

Here k_j and c_j are the wavenumber and the Biésel transfer function, respectively. These are real for $j=0$ and imaginary for $j>0$ representing evanescent modes. For a piston-type wavemaker, we have

$$c_j = \frac{2 \sinh^2 k_j h}{k_j h + \sinh k_j h \cosh k_j h} \tag{13}$$

see e.g. Schäffer (1996) for other types of wavemakers. While $j>0$ gives evanescent modes for any value of p, progressive modes require that $j=0$ and that p is sufficiently small as to get $|k_{yp}|<k$. Singularities appear in the transition from progressive to evanescent modes, since the square root in (12) vanishes when
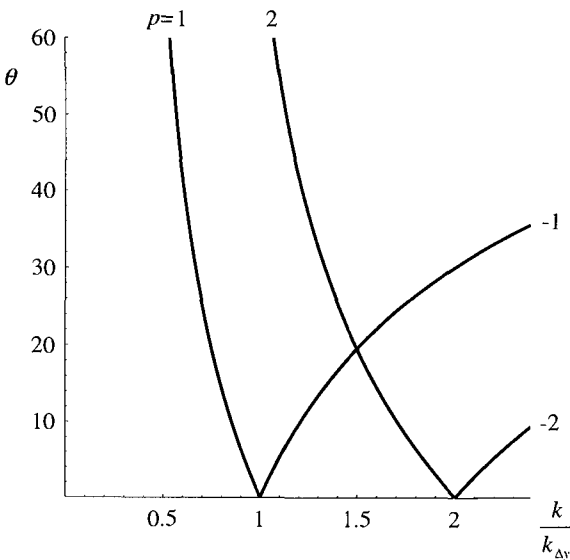

Figure 4. Singularities for spurious wave amplitudes, see (14).

$$\left| p\frac{k_{\Delta y}}{k} - \sin\theta \right| = 1 \tag{14}$$

where θ is the angle between the wavenumber vector and the wavemaker orthogonal. These singularities are shown in Fig. 4 for $p = \pm 1,\ \pm 2$. Swapping signs for p and θ gives the same image but mirrored in the abcissa. The singularity for $p=0$ is outside the range of the figure, since it appears for $\theta = \pm 90°$. Obviously, it is desirable to stay away from the singularities, since at these points the mode in question can be expected to grow until nonlinearity or dissipation put an end to it. A criterion often used in multidirectional wave generation is that no progressive spurious modes should be allowed. This criterion is met (and only met) by staying to the left of the singularity curve for $p=1$ (and for $p=-1$ for negative θ) in Fig.4, i.e. requiring $k/k_{\Delta y} < 1/(1 + \sin|\theta|)$. However, theoretically this may still give arbitrarily high evanescent mode amplitudes and this is one possible source of cross modes sometimes seen to build up near the wavemaker eventually ruining the physical experiment.

For comparison with Fig. 4 and the figures shown later, contours of resolution, $k_y/k_{\Delta y} = 1/2$, 1/5 and 1/10 versus $k/k_{\Delta y}$ and θ are shown in Fig. 5.

Usually, the desired wave is progressive, and omitting the zero's for the subscripts j and p on the wavenumber components, we have

$$\eta_{00}(x, y, t) = A_{00}\exp\left[i(\omega t - k_x x - k_y y)\right],$$
$$A_{00} = \frac{X_a a_0 c_0}{\cos\theta},\quad (k_x, k_y) = k(\cos\theta, \sin\theta) \tag{15}$$
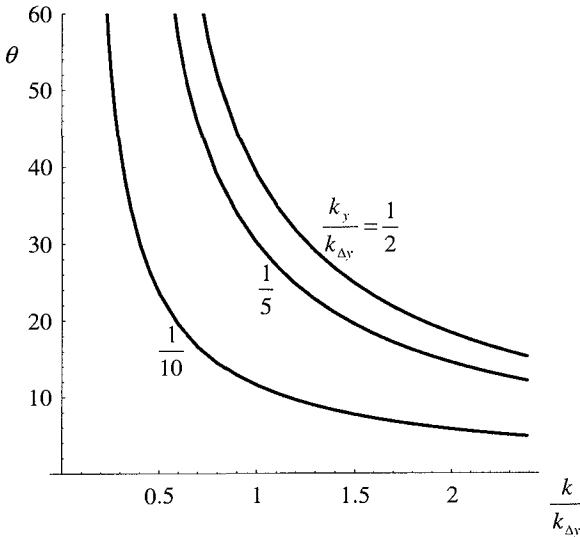

Figure 5. Hyperbolas showing constant resolution.

Sand (1979) concentrated on the number of evanescent modes as well as on the Fourier coefficients for the paddle motion, a_p. However, as pointed out by Christensen (1995), it is rather the magnitude of the resulting waves which is interesting from a wave generation point of view. Generating spurious waves is not a problem as long as their magnitude is sufficiently small. Thus, we look at the amplitude, A_{0p} of the dominant mode ($j=0$) for the p'th spurious wave relative to the desired wave amplitude, A_{00}. From (11), we get

$$\frac{A_{0p}}{A_{00}} = \frac{a_p}{a_0} \frac{\cos\theta}{\sqrt{k^2 - k_{vp}^2}} \tag{16}$$

which is again singular when (14) is satisfied. As a rational criterion for whether or not we should include a given desired wave component in the generation of a multidirectional sea state, we suggest to require

$$\left| A_{0p} / A_{00} \right| \le \varepsilon \tag{17}$$

This requirement should be met for all values of p given some small value of the parameter ε. For each p (17) produces two limiting curves, one on the progressive-wave side of the singularity and one on the evanescent-mode side. Including also the singularities, Fig. 6 shows the results using $\varepsilon = 0.2$ for a constant element wavemaker and $p = \pm 1, \pm 2$. The shading indicates the allowable combination of direction, θ and scaled wavenumber, $k / k_{\Delta y}$. The grouping of curves
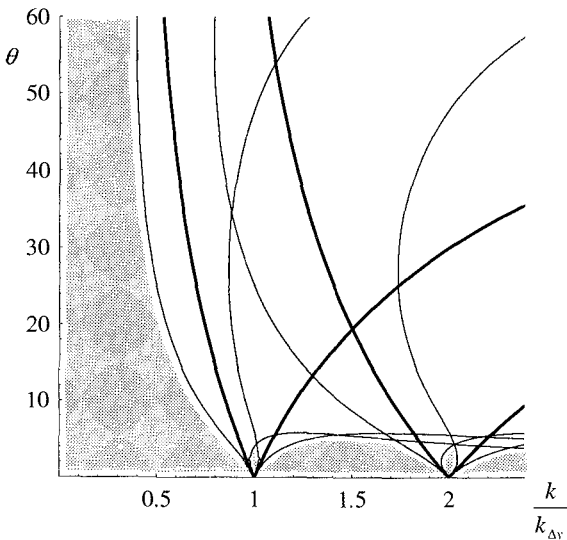

Figure 6. Limiting curves for wave generation defined by (17) with $\varepsilon = 0.2$. Paddle type: constant elements. Thick curves repeat the singularities from Fig. 4.
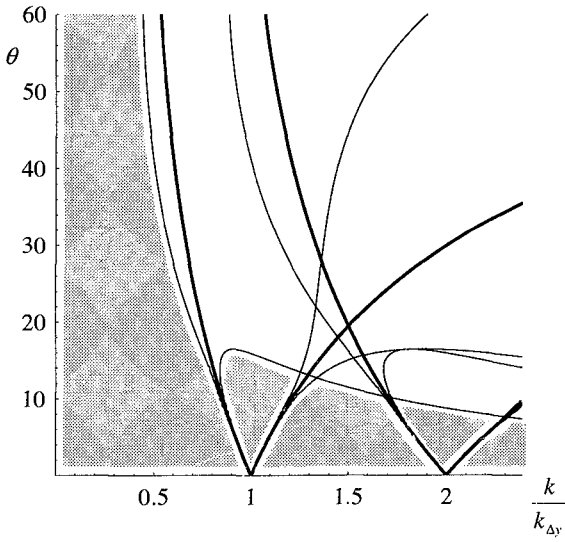
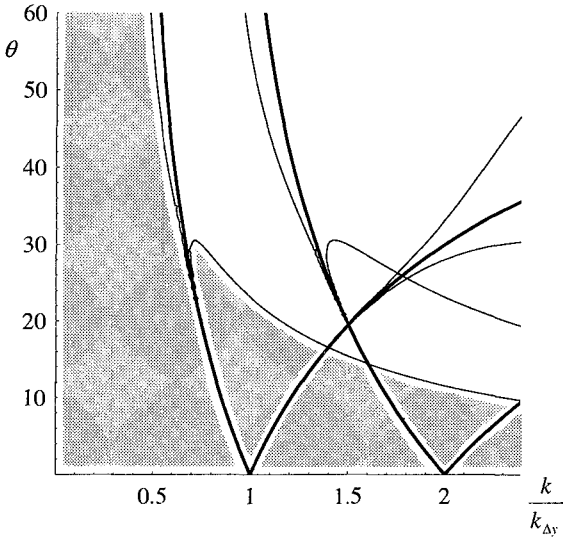Figure 7. As Fig. 6, but for linear elements.

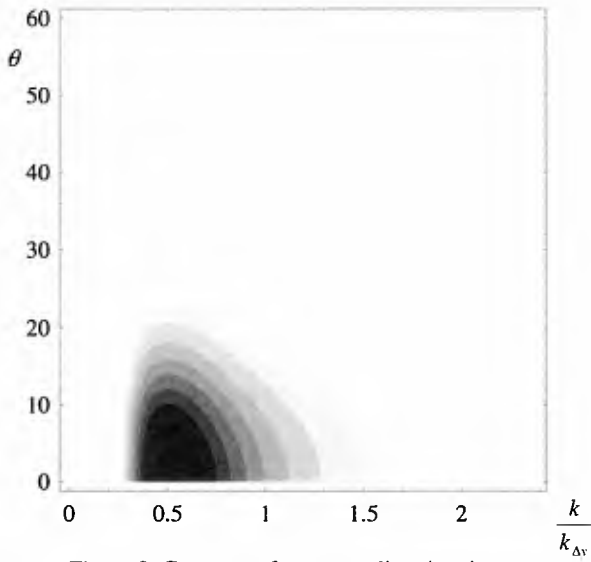Figure 8. As Fig. 6, but for cubic spline elements.

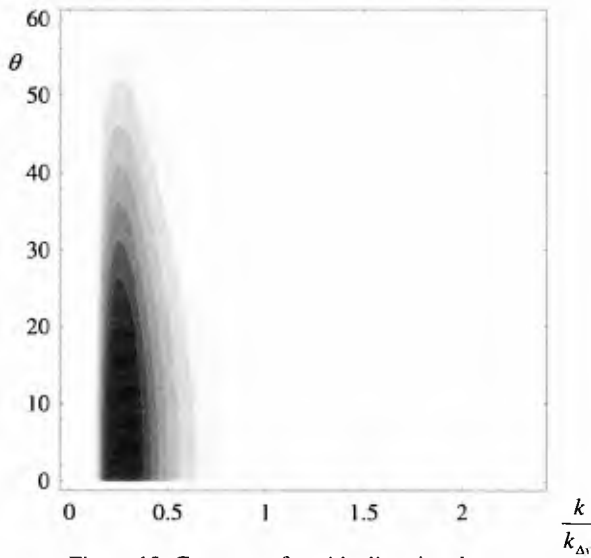Figure 9. Contours of a narrow directional spectrum.

Figure 10. Contours of a wide directional spectrum

in sets of three for each value of p is more evident in Fig. 7 which shows similar results but for linear elements. The range of applicability is somewhat increased, but mainly for small. The limit of what a flexible paddle front could provide is seen in Fig. 8 showing the results for cubic spline elements. Although the improvement is evident, we note that again the advantage is quite small for waves with oblique mean direction.

For comparison with the allowable regions in Figs. 6-8, Figs. 9 and 10 show two examples of directional spectra. For both spectra the frequency variation is a Pierson-Moskowitz spectrum and the directional distribution is proportional to $\cos^{2s}(\theta/2)$. Ten equidistant contours are shown between the directional spectral peak value and zero. In Fig. 9 the directional distribution is quite narrow with $s=40$ corresponding to a directional spread of $\sigma_\theta=13°$. The spectral peak is at $k/k_{\Delta y}=1/2$ e.g. corresponding to a peak frequency f_p at 1.25Hz for a segment width of $\Delta y=0.5$m (using the deep water dispersion relation). In comparison with the allowable regions in Figs. 6-8 it appears that the linear segments show a significant improvement over the constant ones (the staircase approximation) and the cubic splines give yet an improvement. However, shifting the mean direction in Fig. 9 to for example 30°, this advantage disappears as only one side of the directional distribution can be generated. In Fig. 10 the directional distribution is quite wide with $s=6$ ($\sigma_\theta=32°$), while the peak is now at $k/k_{\Delta y}=1/4$ corresponding to $f_p\approx0.88$Hz assuming $\Delta y=0.5$m and deep water theory. For this case the difference between the three types of paddle front is rather small even for zero mean direction.

Spatial Aliasing
Collecting for example surface elevation time series usually involves a discrete sampling of a continuous measurement. In order to avoid aliasing, a suitable lowpass filter is applied to the analogue signal before the digital sampling takes place. The situation is quite different when measuring the surface elevation at equidistant points along the wavemaker. In this case, the surface elevation is sampled directly in discrete space. Thus, no underlying continuous measurement is available for eliminating aliasing in the sampling process. Assuming that the sampling interval equals the segment width, aliasing takes place for $L_y/\Delta y<2$, (equivalent to the Nyquist frequency). Aliasing wraps wavenumbers k_y to

$$\tilde{k}_y = k_y + nk_{\Delta y} \tag{18}$$

where n is determined so that

$$-\frac{k_{\Delta y}}{2} < \tilde{k}_y < \frac{k_{\Delta y}}{2} \tag{19}$$

Assuming that k_y is inside the Nyquist range, the spurious wavenumbers $k_{yp} = k_y - pk_{\Delta y}$ given in (9) are all outside this range and aliasing wraps them back to get $\tilde{k}_{yp} = k_y$. Naturally, sampling the Fourier series for the paddle position (9), the original expression in (2) recovers as can be confirmed by checking that for all types of elements we have

$$\sum_{p=-\infty}^{\infty} a_p = 1 \tag{20}$$

For the surface elevation in (11), however, the transfer function e_{jp} modifies the terms in the summation so that the sampled elevation varies with type of element. This modification, however, is not a problem as it can be easily computed.

Other sources of short waves contaminating the system through aliasing must be anticipated. Nonlinearity is bound to give higher harmonics, both directly in the wave generation itself and indirectly through reflections from possible fixed or floating structures. Since the waves from these sources are unknown, we are not able to compensate for their influence. Consequently, a 3D active absorption system based on a discretely spatially sampled surface elevation will misinterpret very short waves as longer waves and thus try to absorb these longer waves, which do not exist. In this attempt, the system will generate unwanted waves.

Since the surface elevation is sampled both in space and time, the dispersion relation in principle makes it possible to overcome the spatial aliasing by lowpass filtering in the time domain. The frequency domain transfer function of such a lowpass filter transforms into the wavenumber domain, k. However, the desired effect is to restrict energy to small values of the wave number projection, k_y. Since for progressive waves $k \geq k_y$ the aliasing problem can be solved by eliminating frequencies for which $L/\Delta y < 2$ (or $k/k_{\Delta y} > 1/2$), where $L = 2\pi/k$ is the wave length. Unfortunately, this requires a quite severe filtering, which we have found to impose unacceptable limits to the range of application for the active absorption system. Note, however, that wave generation and active absorption can be separated so that the filtering only affects the active absorption range and not the generation range.

In search for other means of reducing the potential problem of aliasing, we examine the effect of spatial averaging between consecutive surface elevation gauges. Let the gauge distance equal the segment width and let each gauge be centred between two control points, i.e. at $y = (m+1/2)\Delta y$. (This arrangement is not feasible for constant elements, as the paddle position is discontinuous at these points.) Spatial averaging between two gauge signals is equivalent to a multiplication in the k_y domain by the transfer function

$$H_1(k_y \Delta y) = \cos\left(\frac{k_y \Delta y}{2}\right) \tag{21}$$

as depicted in Fig. 6a. This is a notch filter, which has the desirable property that it removes all energy at the Nyquist wavenumber $k_y/k_{\Delta y} = 1/2$ (and uneven multiples of 1/2), and the undesirable property of no reduction of energy for integer values of $k_y/k_{\Delta y}$. In combination with this spatial averaging, the time domain lowpass filtering as mentioned above can be less restrictive with a slightly higher cut-off frequency. However, as we still do not find this combination satisfactory, we shall investigate the consequences of doubling the number of surface elevation gauges placing these at $y = (m+1/2)\Delta y/2$. Aliasing now follows (18) and (19) with $\Delta y/2$ in place of Δy and spatial average among two neighbouring gauges corresponds to the transfer function

$$H_2(k_y \Delta y) = \cos\left(\frac{k_y \Delta y}{4}\right) \tag{22}$$

as shown in Fig. 6b. Combining (21) and (22), we get

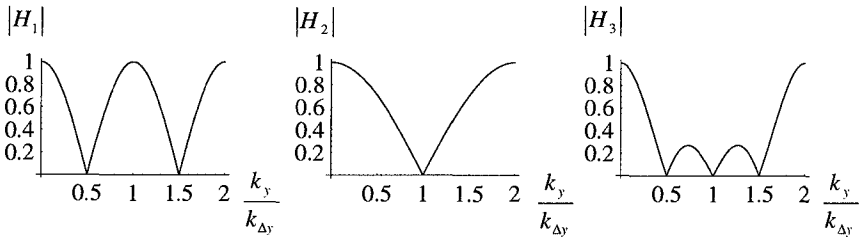$|H_1|$ $|H_2|$ $|H_3|$

Figure 11. Transfer functions (21)-(23) for spatial averaging reducing aliasing problems.

$$H_3(k_y\Delta y) = \cos\left(\frac{k_y\Delta y}{2}\right)\cos\left(\frac{k_y\Delta y}{4}\right) = \frac{1}{2}\cos\left(\frac{k_y\Delta y}{3}\right) + \frac{1}{2}\cos\left(\frac{k_y\Delta y}{4}\right) \quad (23)$$

Here the first version is given by $H_3=H_1H_2$ as obtained by two consecutive spatial averages between two neighbouring values, while the second formulation is found by considering the process as one spatial average between four neighbouring gauges. By this combination, we have obtained a stop band as seen in Fig. 6c. Consequently the supporting time domain filter can use a much higher and less restrictive cut-off frequency and still significantly reduce the contamination of the active absorption system due to short-wave aliasing. This solution has been chosen for the new multidirectional wavemaker under construction at DHI. A more elaborate analysis involving variable coefficients in the spatial averages did not show an overall improvement.

CONCLUSIONS

With regard to the type of wavemaker paddle front (Fig. 1) no differences appear in the limitations for multidirectional wave generation if the traditional cut-off in frequency and direction is used i.e. requiring no *progressive* spurious waves. A more elaborate criterion has been proposed, which reduces the application range slightly for very oblique waves in order to avoid large evanescent spurious waves. These could be the source of destructive cross modes and would in particular be unwanted when using surface elevation signals at the paddle front for hydrodynamic feedback to and active absorption system. On the other hand the new criterion permits a wider frequency range for very small obliqueness and increasingly much so for the more sophisticated segment type.

   Both progressive and evanescent spurious waves should be recognized in surface elevation measurements at the paddle front for active absorption. In this connection aliasing of short-wave energy due to finite segment width and in particular due to other sources should be recognized. Means of reducing the aliasing problem have been discussed. A combination of better spatial resolution of elevation measurements and time-domain low-pass filtering in the active absorption system is suggested.

REFERENCES

Christensen, M. (1995). *Generation and active absorption of 2- and 3-dimensional linear water waves in physical models.* PhD Thesis. Series paper **11**, Hydraulics & Coastal Engng. Lab, Aalborg University, 90 pp.

Dean, R.G. and R.A. Dalrymple (1984). Water wave mechanics for engineers and scientists. Prentice Hall.

Sand, S.E. (1979). Three-dimensional deterministic structure of ocean waves. PhD Thesis. Series paper 24, Inst. Hydrodyn. and Hydr. Engng. (ISVA), Tech. Univ. of Denmark, 177 pp.

Schäffer, H.A. and J. Skourup (1996). Active absorption of multidirectional waves. Proc. 25th Int. Conf. on Coastal Engng., Orlando, FL, USA, pp 55-66.

Schäffer, H.A. and G. Klopman (1997). Review of multidirectional active wave absorption methods. Proc. IAHR-Siminar: Multidirectional Waves and their Interaction with Structures, San Francisco, CA, USA, pp 131-158. Also submitted to J. Waterway, Port, Coastal and Ocean Engng.